

# CoFiI2P: Coarse-to-Fine Correspondences for Image-to-Point Cloud Registration

Shuhao Kang\*, Youqi Liao\*, Jianping Li<sup>†</sup> *Member, IEEE*, Fuxun Liang, Yuhao Li, Fangning Li, Zhen Dong  
*Member, IEEE*, Bisheng Yang<sup>†</sup>

**Abstract**—Image-to-point cloud (I2P) registration is a fundamental task in the fields of robot navigation and mobile mapping. Existing I2P registration works estimate correspondences at the point-to-pixel level, neglecting the global alignment. However, I2P matching without high-level guidance from global constraints may converge to the local optimum easily. To solve the problem, this paper proposes CoFiI2P, a novel I2P registration network that extracts correspondences in a coarse-to-fine manner for the global optimal solution. First, the image and point cloud are fed into a Siamese encoder-decoder network for hierarchical feature extraction. Then, a coarse-to-fine matching module is designed to exploit features and establish resilient feature correspondences. Specifically, in the coarse matching block, a novel I2P transformer module is employed to capture the homogeneous and heterogeneous global information from image and point cloud. With the discriminate descriptors, coarse super-point-to-super-pixel matching pairs are estimated. In the fine matching module, point-to-pixel pairs are established with the super-point-to-super-pixel correspondence supervision. Finally, based on matching pairs, the transform matrix is estimated with the EPnP-RANSAC algorithm. Extensive experiments conducted on the KITTI dataset have demonstrated that CoFiI2P achieves a relative rotation error (RRE) of 2.25 degrees and a relative translation error (RTE) of 0.61 meters. These results represent a significant improvement of 14% in RRE and 52% in RTE compared to the current state-of-the-art (SOTA) method. The demo video for the experiments is available at <https://youtu.be/TG2GBrJTUw4>. The source code will be public at <https://github.com/kang-1-2-3/CoFiI2P>.

**Index Terms**—Image-to-point cloud registration, coarse-to-fine correspondence, transformer

## I. INTRODUCTION

This study was jointly supported by the National Natural Science Foundation Project (No. 42130105, No. 42201477), China Postdoctoral Science Foundation (2022M712441, 2022TQ0234), and Open Fund of Key Laboratory of Urban Spatial Information, Ministry of Natural Resources (Grant No. 2023ZD001). (Shuhao Kang and Youqi Liao are co-first authors.) (Corresponding authors: Jianping Li and Bisheng Yang)

Shuhao Kang is with LIESMARS, Wuhan University, Wuhan 430079, China, and the school of Engineering and Design, Technical University of Munich, 80333 Munich, Germany (e-mail: shuhao.kang@tum.de).

Youqi Liao and Zhen Dong are with the Hubei Luoqia Laboratory, Wuhan University, Wuhan 430079, China and also with the LIESMARS, Wuhan University, Wuhan 430079, China (e-mail: martin\_liao@whu.edu.cn, dongzhenwhu@whu.edu.cn).

Jianping Li is with the School of Electrical and Electronic Engineering, Nanyang Technological University, 50 Nanyang Avenue 639798, Singapore. (e-mail: jianping.li@ntu.edu.sg).

Fangning Li is with Beijing Urban Construction Exploration and Surveying Design Research Institute Co. Ltd, Beijing 100101, China. (e-mail: 64877558@qq.com)

Fuxun Liang, Yuhao Li and Bisheng Yang is with the LIESMARS, Wuhan University, Wuhan 430079, China. (e-mail: liangfuxun@whu.edu.cn, yhaoli@whu.edu.cn, bshyang@whu.edu.cn).

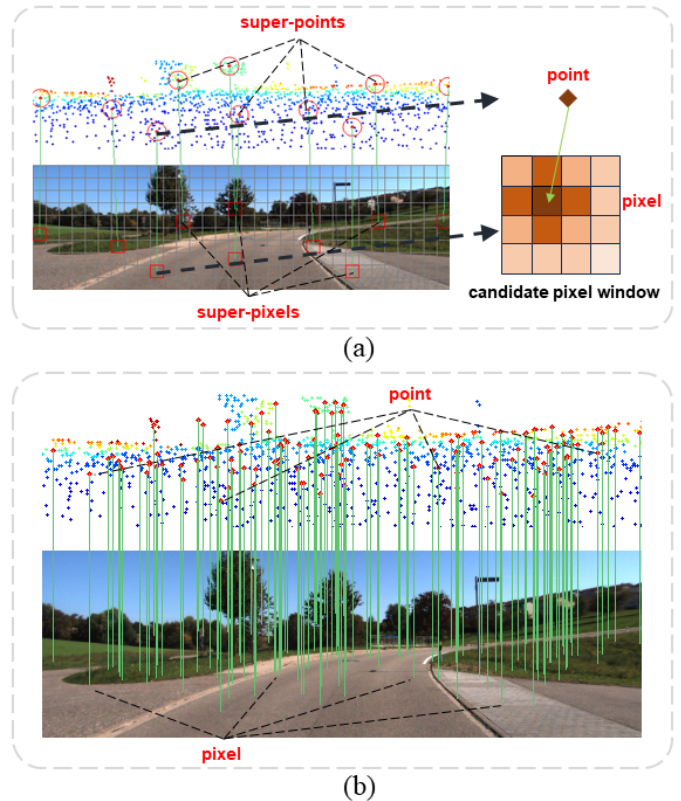


Fig. 1. Comparison of the proposed coarse-to-fine I2P registration scheme and the existing one-stage I2P registration scheme. (a) shows the coarse-to-fine two-stage registration pipeline. Darker color represents higher similarity between the node point and the candidate pixel. (b) shows the one-stage registration pipeline

**E**stimating six degrees of freedom (6-DoF) pose of a monocular image with respect to a pre-build point cloud map is a fundamental requirement for robot navigation [1, 2], re-localization [3, 4] and mobile mapping [5]. An accurately estimated relative transformation leads to well fusion of the multi-modal information between the images and pre-build point cloud maps, e.g. segmentation[6], detection [7], autonomous driving [8, 9], and change detection for map update [10]. Specifically, the low-cost unmanned ground vehicle (UGV) only equipped with a monocular camera suffers from scale ambiguity in absolute localization and depth sensing.

However, cross-modality registration has its inherent challenges. Some existing methods use hand-crafted detectors and descriptors for I2P registration [11, 12]. These approaches

rely on structured features like edge or line features [11, 13], which are limited by specific environmental conditions. With the rapid development of deep learning (DL), learning-based I2P registration approaches [14, 15, 16] have been proposed to extract representative keypoints and descriptors. 2D3D-Matchnet [14] is the first learning-based I2P registration approach, which extracts SIFT [17] and ISS [18] keypoints from image and point cloud as registration primitives, respectively. Then it learns the descriptors with convolution neural networks (CNN). However, the manually designed detectors for keypoints extraction lead to poor in-frustum correspondence accuracy. To alleviate the difficulty of correspondence construction and improve the registration success rate, DeepI2P [15] converts the registration problem to a classification problem. A novel binary classification network is designed to distinguish whether the projected points are within or beyond the camera frustum. The classification results are passed into an inverse camera projection solver to estimate the transformation between the camera and laser scanners. As a large number of points on the boundary are misclassified, the accuracy of the camera pose is still limited. CorrI2P [16] proposed an overlap region detector for both image and point cloud, then pixels and points in the overlap region are matched to obtain I2P correspondences. Feature fusion module is exploited to fuse the point cloud and image information. Although CorrI2P [16] has significant improvement over DeepI2P [15], matching merely on one stage, namely, the pixel-point level without global alignment guidance, can lead to local minimal and instability. Fig. 1 illustrates the difference between the coarse-to-fine matching scheme and the existing one-stage matching scheme. Moreover, the feature fusion module used in the existing I2P method simply transfers the global features to another modality, where the long-range context in same-modality and cross-modality data is ignored.

Inspired by recent coarse-to-fine matching schedules and transformers in image-to-image (I2I) registration [19, 20] and point cloud-to-point cloud (P2P) registration approaches [21, 22], this paper proposes **Coarse-to-Fine Image-to-Point cloud (CoFiI2P)** network to tackle the challenges of existing one-stage I2P registration. I2P transformer with self-attention modules and cross-attention modules is embedded into the network for global alignment. CoFiI2P mainly contains four modules: feature extraction (FE), coarse matching (CM), fine matching (FM), and pose estimation (PE). We employ CNNs as FE backbone to extract hierarchical features from image and point cloud. With the U-Net [23] like structure, local features are concatenated with global features by skip connections for each pixel and point. Then CM and FM modules utilize multi-scale features extracted from FE to establish coarse-level correspondences first and evolve the fine-level correspondences. Specifically, in the coarse matching (CM) part, the proposed I2P transformer blocks with self-attention and cross-attention are employed to enhance the long-range context and cross-modality response. After the transformer blocks, the resulting 3D super-point and 2D super-pixel carry global-aware information. In the fine matching (FM) part, taking the super-point-to-super-pixel correspondences from CM as input, point-to-pixel correspondences are generated with a pyramid-

matching strategy. In the PE module, the relative transformation between the camera and laser scanners is estimated with EPnP-RANSAC [24, 25]. The main contributions of this paper are as follows:

- 1) A novel coarse-to-fine I2P registration network is proposed to align image and point cloud in a progressive way. The coarse matching step provides robust but rough super-point-to-super-pixel correspondences for the fine matching step, which filters out most mismatched pairs and reduces the computation burden. The fine matching step achieves accurate and reliable point-to-pixel correspondences within the global guidance.
- 2) A novel I2P transformer is proposed, which contains both the self-attention module capturing space context for same-modality data and the cross-attention module extracting hybrid features for image and point cloud data.

The rest of the paper is organized as follows. Section II reviews the existing I2I, P2P and I2P registration works. Section III elaborates on the network design of CoFiI2P. Extensive experiments are conducted in Section IV. Section V discusses the crucial module and false registration cases in the experiments. Conclusion and future work are drawn in Section VI.

## II. RELATED WORK

### A. Same-modality Registration

**I2I Registration:** Before the age of deep-learning, hand-crafted detectors and descriptors (i.e., SIFT [17] and ORB [26]) are widely used to extract correspondences. Compared to traditional methods, learning-based methods improve the robustness and accuracy of image matching with large viewpoint differences and illumination changes. MagicPoint [27] proposed a point-tracking system powered by two CNNs. The first network in MagicPoint detects salient points and the second network estimates the transformation relationship. Based on MagicPoint, SuperPoint [28] proposed a self-learning training method through homography adaptation. SuperGlue [29] proposed an attention-based graph neural network (GNN) for feature matching. Patch2Pix[30] is the first work to obtain patch matches and regress pixel-wise matches in a coarse-to-fine manner. Cotr [20] proposed a hybrid transformer and CNN network that applies to both coarse and dense matching problems. LoFTR [19] operates detector-free matching to get dense correspondences and overcomes small receive field of CNN with transformer. However, I2I registration methods can not be directly transferred to the I2P registration task, which should extract heterogeneous features from cross-modality data.

**P2P Registration:** Point cloud registration aims to estimate the optimal rigid transformation of two point clouds. Correspondence-based methods [31, 32, 33] estimate the correspondence first and recover the transformation with robust estimation methods[25]. RoReg [22] embeds orientation information of point cloud to estimate local orientation and refine coarse rotation through residual regression to achieve fine registration. In the transformer era, point-based transformers

[21, 34, 35] have emerged and shown great performance. CoFiNet [36] followed LoFTR’s [19] design and proposed coarse-to-fine correspondences for registration, which computed coarse matches with descriptors strengthened by the transformer and refined coarse matches through density adaptive matching module. REGTR [37] predicts overlap point sets and directly outputs transformed points to estimate transformation. PREDATOR [38] first predicts the overlap region between two point clouds and finds corresponding points with overlap scores and matching ability scores. GeoTransformer [21] proposed a geometric Transformer to make full use of the 3D properties of the point cloud. BUFFER [35] proposed an efficient, accurate and generalized network that utilizes both point-wise and patch-wise information for registration. As the point cloud and image are cross-modality data, which are characterized by totally different information, above same-modality registration methods cannot be directly applied.

### B. Cross-modality Registration

To address the cross-modality registration problem, a variety of I2P registration methods have been proposed, which could be roughly divided into two categories: I2P fine registration (initial transformation dependent) and I2P coarse registration (initial transformation free). The I2P fine registration methods [5, 39, 40, 41] rely on initial transform parameters, and are widely applied in sensors calibration. Although this paper focuses on the second class, namely the coarse I2P registration without any initial transformation knowledge, we give an exhaustive review of both categories registration methods here.

**Fine registration methods:** Fine registration methods have been thoroughly researched for several decades. Early-stage studies [42, 43, 44] utilize various artificial targets as calibration constraints. In recent years, some approaches have argued that structured features shared in images and point cloud could be used for target-less I2P registration, e.g., edge feature [45] and line feature [11, 12]. Stamos et al. [45] computes orientation with vanishing points and then calculates camera position by matching 2D and 3D line features. Pandey et al. [46] uses mutual information (MI) as the registration criterion to automatically align a 3D laser scanner and camera. Zhang et al. [11] proposed a line-based method to register image and point cloud. Levinson and Thrun [39] employs edge information and optimizes transformation according to the response value. Recently, research on 2D and 3D semantic segmentation motivates semantic feature-based I2P registration. Li et al. [5] extracts vehicles from panoramic image and point cloud and maximizes the overlapping area through Particle Swarm Optimization (PSO) to achieve accurate transformation estimation. Liao et al. [41] further studied semantic edges in I2P registration to employ more common semantic information instead of a certain type of object. Overall, fine registration methods achieve high registration accuracy but rely on initial transform knowledge.

**Coarse registration methods:** 2D3D-Matchnet [14] is the pioneering method to regress the relative transform parameters with CNN. It extracts SIFT [17] and ISS [18] keypoints from image and point cloud and learns descriptors with a

Siamese network. However, the hand-crafted detectors from different modalities match poorly. DeepI2P [15] proposed a feature fusion module to merge image and point cloud information and classify points in/beyond the camera frustum. CorrI2P [16] predicts pixels and points in overlapping areas and matches with dense per-pixel/per-point features directly to get I2P correspondences. Although overlapping region detectors significantly reduce the number of false candidates, I2P registration only using the low-level feature without global guidance leads to too many mismatches. Inspired by the coarse-to-fine strategies in CoFiNet [36], we propose the coarse-to-fine I2P registration network CoFiI2P, which injects the high-level response information into low-level matching for rejecting mismatches.

## III. METHODOLOGY

For convenient description, a pair of partially overlapped image and point cloud are defined as  $I \in \mathbb{R}^{W \times H \times 3}$  and  $P \in \mathbb{R}^{N \times 3}$ , where  $W$  and  $H$  are the width and height, and  $N$  is the number of points. The purpose of I2P registration is to estimate the relative transformation between the image  $I$  and point cloud  $P$ , including rotation matrix  $R \in SO(3)$  and translation vector  $t \in \mathbb{R}^3$ .

Our method adopts the coarse-to-fine manner to find the correct correspondences set  $\Omega(I, P)$ . The CoFiI2P mainly consists of four modules: feature extraction (FE), coarse matching (CM), fine matching (FM) and pose estimation (PE). FE is an encoder-decoder structure network, which encodes raw inputs from different modalities into high-dimension feature spaces. CM and FM are cascaded two-stage matching modules. CM constructs coarse matching at super-pixel/super-point level, and then FM constructs fine matching at pixel/point level sequentially with super-pixel/super-point correspondences’ guidance. Lastly, the PE module exploits point-pixel matching pairs to regress the relative transform with the EPnP-RANSAC [24, 25] algorithm. Workflow of the proposed method is shown in Fig. 2.

### A. Feature extraction

We utilize ResNet-34 [47] and KPConv-FPN [48] as the backbones for image and point cloud to extract multi-level features. The encoder progressively compacts raw inputs into high-dimensional features, and the decoder propagates high-level information to low-level details with skip-connection for dense per-pixel/point feature generation. [49, 50] have shown that the skip-connect design could combine the details and semantic information for dense prediction. Therefore, we extract representative features from multiple resolutions for coarse-to-fine matching. Specifically, super-points set  $\tilde{P}$  and super-pixels set  $\tilde{I}$  at the coarsest resolution are chosen as candidates for coarse matching. The associated features for super-points and super-pixels are denoted as  $F_{\tilde{P}} \in \mathbb{R}^{n \times C}$  and  $F_{\tilde{I}} \in \mathbb{R}^{|\tilde{wh}| \times C}$ , where  $n, w, h, C$  mean the number of super-points, width, height and dimension of superpixels’ feature map.

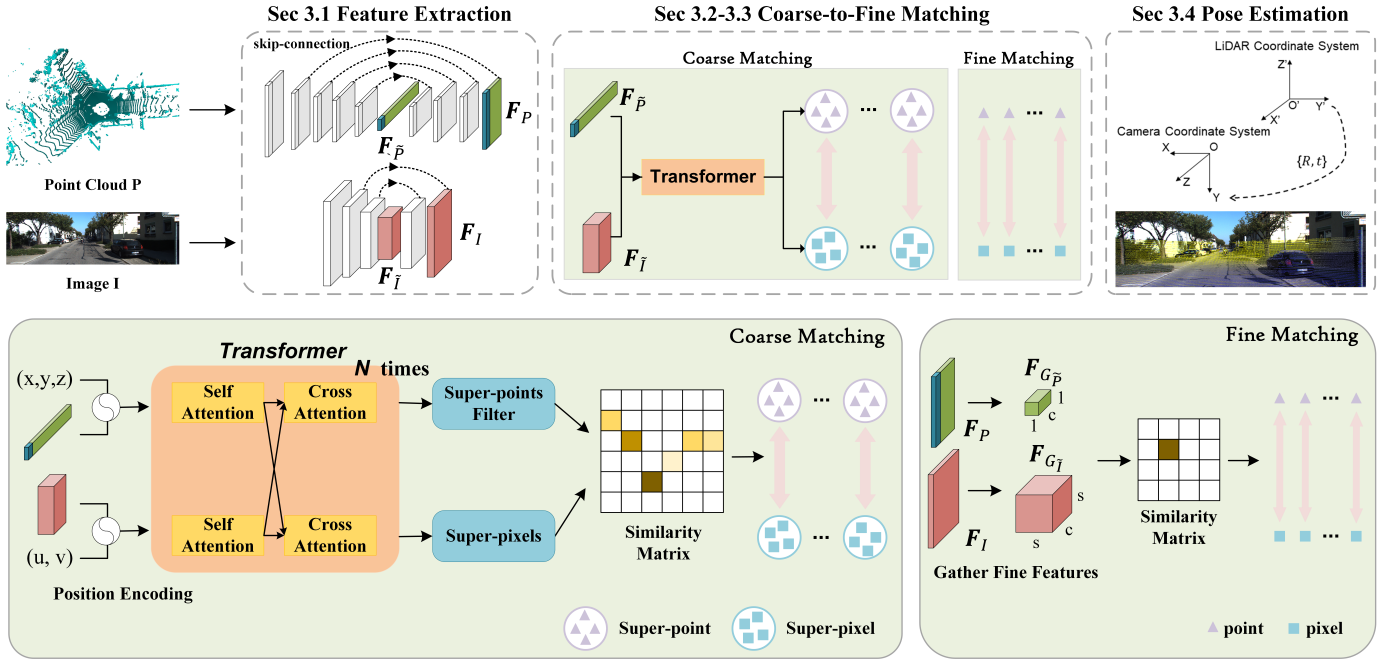


Fig. 2. Workflow of CoFil2P. The proposed method consists of feature extraction, coarse matching, fine matching and pose estimation modules. Image and point cloud are sent to the feature extraction module to obtain hierarchical deep features, respectively. The coarse-level features are strengthened by I2P transformer module and then matched with the cosine similarity rule. Fine features are gathered from the last layer of the decoder. In each super-point-to-super-pixel pair, the node point is set as the candidate and the corresponding pixel is selected from the super-pixel area, a  $s \times s$  window. The generated dense matching pairs are utilized to regress the pose with the EPnP-RANSAC [24, 25] algorithm.

For each super-point  $\tilde{p}$ , the local patch points  $G_{\tilde{p}}$  around it for point cloud convolution are constructed with the point-to-node strategy in the feature space:

$$G_{\tilde{p}} = \{p_x \in P \mid \|p_x - \tilde{p}\| < r_g\}, \quad (1)$$

where  $r_g$  is the chosen radius. As the pixels array on the image with a rigid order, the local patch pixels  $G_{\tilde{i}}$  construct simply with the pyramid matching strategy.

### B. Coarse Matching

In CM module, I2P transformer is utilized to capture the geometric and spatial consistency between image and point cloud. Each stage of the I2P transformer consists of a self-attention block for inter-modality long-range context and a cross-attention module for intra-modality feature exchange. The self-attention and cross-attention modules are repeated  $N$  times to extract well-mixed features for super-point-to-super-pixel matching.

**I2P Transformer:** [51, 52] have shown that Vision Transformer (ViT) outperforms traditional CNN-based methods with a large margin in classification, detection, segmentation and other tasks. Furthermore, recent approaches [19, 20, 34] have introduced transformer modules for I2I and P2P registration tasks. Therefore, we introduce the I2P transformer module customized for cross-modality registration task to enhance the representability and robustness of descriptors. Different from ViT used in the same-modality registration tasks, our I2P transformer contains both self-attention modules for space context capturing in homogeneous data and cross-attention for hybrid feature extraction among heterogeneous data.

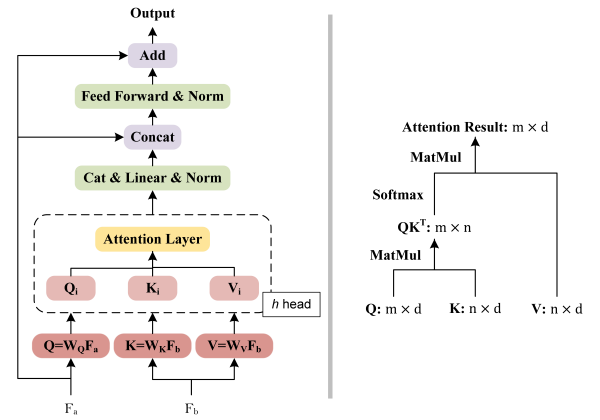


Fig. 3. Illustration of I2P Transformer module (left) and attention module (right)

For the self-attention module, given a coarse-level feature map  $F \in \mathbb{R}^{n \times C}$  of image or point cloud, the query, key and value vectors  $q, k, v$  are generated as:

$$q = W_q F, k = W_k F, v = W_v F, \quad (2)$$

where  $W_q, W_k \in \mathbb{R}^{C_{qk}^{sa} \times C}$ ,  $W_v \in \mathbb{R}^{C_v^{sa} \times C}$  are learnable weight matrixs, as shown in Fig. 3. Then, the global attention is calculated as:

$$F^{sa} = \text{Softmax}\left(\frac{qk^T}{\sqrt{C}}\right)v. \quad (3)$$

Extracted global-aware features  $F^{sa}$  are fed into the feed-forward network (FFN) to fuse the spatial relation information

in channel dimension. Given a feature map  $F$ , the relative positions are encoded with multi-layer perception (MLP) [53].

Cross-attention is designed for fusing image and point cloud features in I2P registration task. Given the self-attention feature map  $\mathbf{F}_{\tilde{P}}^{sa}, \mathbf{F}_{\tilde{I}}^{sa}$  for super-points set  $\tilde{P}$  and super-pixels set  $\tilde{I}$ , cross-attention features  $\mathbf{F}_{\tilde{P}}^{ca}$  of point cloud and  $\mathbf{F}_{\tilde{I}}^{ca}$  of image are calculated as:

$$\begin{aligned}\mathbf{F}_{\tilde{P}}^{ca} &= \text{Softmax}\left(\frac{\mathbf{q}_{\tilde{P}}\mathbf{k}_{\tilde{I}}^T}{\sqrt{C}}\right)\mathbf{v}_{\tilde{P}}, \\ \mathbf{F}_{\tilde{I}}^{ca} &= \text{Softmax}\left(\frac{\mathbf{q}_{\tilde{I}}\mathbf{k}_{\tilde{P}}^T}{\sqrt{C}}\right)\mathbf{v}_{\tilde{I}},\end{aligned}\quad (4)$$

where  $\mathbf{q}_{\tilde{P}}, \mathbf{k}_{\tilde{P}}, \mathbf{v}_{\tilde{P}}$  are query, key and value vectors of point cloud feature  $\mathbf{F}_{\tilde{P}}^{sa}$ , and  $\mathbf{q}_{\tilde{I}}, \mathbf{k}_{\tilde{I}}, \mathbf{v}_{\tilde{I}}$  are query, key and value vectors of image feature  $\mathbf{F}_{\tilde{I}}^{sa}$ .

While self-attention module encodes the spatial and geometric features for each super-pixel and super-point, the cross-attention module injects the geometric structure information and texture information across image and point cloud respectively. Outputs of the I2P transformer carry powerful cross-modality information for matching.

**Super-point/Super-pixel Matching:** For monocular camera, the field of view (FoV) is obviously smaller than the laser scans of 3D Lidar (e.g., Velodyne-H64), which usually sweeps 360 degrees in the horizontal direction. Therefore, only a small number of super-points are in the camera frustum. To filter out beyond-frustum super-points, we add a simple binary classification head to predict super-points in or beyond the frustum of the camera. After the beyond-frustum super-points are removed, the distance matrix between candidate super-points and super-pixels in feature space is calculated. Given a defined super-points set  $\tilde{P}$  and super-pixels set  $\tilde{I}$ , the super-point-to-super-pixel corresponding set  $\tilde{\Omega}_{\mathcal{M}}(I, P)$  is defined by sorting the nearest super-pixel  $\tilde{i}$  for each in-frustum super-point  $\tilde{p}$  in feature space:

$$\tilde{\Omega}_{\mathcal{M}} = \{(\tilde{p}_x \in \tilde{P}, \tilde{i}_y \in \tilde{I}) | y = \underset{|\tilde{I}|}{\text{argmin}} \|\mathbf{F}_{\tilde{P}}^{ca}(\tilde{p}_x) - \mathbf{F}_{\tilde{I}}^{ca}(\tilde{i}_y)\|\}.\quad (5)$$

### C. Fine Matching

The first-stage matching at a coarse level constructs coarse super-pixels and super-points pairs  $\tilde{\Omega}_{\mathcal{M}}$  but leads to poor registration accuracy. In order to obtain high-quality I2P correspondences, we generate fine correspondence based on the coarse matching results. During the decoder process, in each super-point/super-pixel correspondence  $(\tilde{p}, \tilde{i})$ , the super-point  $\tilde{p}$  reverse to  $\frac{N}{n}$  points and the super-pixel  $\tilde{i}$  reverse to  $\frac{W}{w} \times \frac{H}{h}$  pixels. Considering the uneven distribution of point cloud and computational efficiency, only the node points  $p_n$  in local patch group  $G_{\tilde{p}}$  are selected to establish correspondences. For each node point  $p_n$ , we select the pixel  $i_k \in \tilde{i}$  that lies nearest in the feature space. Point-pixel pairs in each super-point-super-pixel pair are concatenated together to form the dense corresponding pairs  $\Omega_{\mathcal{M}}$ . With point feature map  $\mathbf{F}_{G_{\tilde{p}}}$

and pixel feature map  $\mathbf{F}_{G_{\tilde{i}}}$  of local patch, the whole fine matching process is defined as:

$$\begin{aligned}\Omega_{\mathcal{M}} &= \{(p_n \in G_{\tilde{p}}, i_k \in G_{\tilde{i}}) | \\ & k = \underset{|G_{\tilde{i}}|}{\text{argmin}} \|\mathbf{F}_{G_{\tilde{p}}}(p_n) - \mathbf{F}_{G_{\tilde{i}}}(i_k)\|\}.\end{aligned}\quad (6)$$

### D. Pose Estimation

With the dense point-pixel pairs  $\Omega_{\mathcal{M}}$ , the relative transformation can be solved with EPnP [24] algorithm. As mentioned in previous approaches, wrong matching may infiltrate into the point-pixel pairs and decrease the registration accuracy. In the CoFiI2P, EPnP-RANSAC [24, 25] algorithm is used for robust estimating camera relative pose.

### E. Loss Function

The loss function  $L = L_{classify} + L_{coarse} + L_{fine}$  consists of  $L_{classify}$  for in/beyond frustum super-points classification,  $L_{coarse}$  for coarse-level descriptors learning, and  $L_{fine}$  for fine-level descriptors learning. Contrastive loss is used to supervise the coarse and dense level descriptor learning, and binary cross-entropy (BCE) loss is used to supervise the in/beyond frustum classification. The similarity  $s(i, p)$  in feature space of image feature  $\mathbf{F}_i$  and point cloud feature is defined as  $\mathbf{F}_p$ :

$$s(i, p) = \frac{\langle \mathbf{F}_i, \mathbf{F}_p \rangle}{\|\mathbf{F}_i\| \|\mathbf{F}_p\|},\quad (7)$$

and the distance  $d(i, p)$  is defined as:

$$d(i, p) = 1 - s(i, p).\quad (8)$$

On the coarse level, the positive anchor  $\tilde{i}_{pos}$  for each in-frustum super-point  $\tilde{p}$  is sampled from the ground-truth pairs set  $\tilde{\Omega}_{\mathcal{M}^*}$ :

$$\tilde{\Omega}_{\mathcal{M}^*} = \{(\tilde{p}_x^* \in P, \tilde{i}_y^* \in I) | \tilde{i}_y^* = \Gamma(\mathbf{T}\tilde{p}_x^*)\},\quad (9)$$

where  $\mathbf{T}$  is the transform matrix from point cloud coordinate system to image frustum coordinate system:

$$\mathbf{T} = \begin{bmatrix} \mathbf{R} & \mathbf{t} \\ \mathbf{0}^T & 1 \end{bmatrix},\quad (10)$$

and  $\Gamma$  represents the mapping function that converts points from camera frustum to image plane coordinate system. For the negative anchor, we followed the CorrI2P [16] to select the negative super-pixel  $\tilde{i}_{neg}$  lies nearest to the  $\tilde{p}$  but farther than a safe radius  $r$ :

$$\tilde{i}_{neg} = \underset{\tilde{i} \in \tilde{P}}{\text{argmin}} \|d(\tilde{i}, \tilde{p})\| \quad \text{s.t.} \quad d(\tilde{p}, \tilde{i}_{neg}) > r.\quad (11)$$

Coarse level descriptor loss is defined in a triplet way:

$$\begin{aligned}L_{coarse} &= \sum_{(\tilde{p}_x, \tilde{i}_y)} [\max(0, d(\tilde{i}_y, \tilde{p}_x) - \Delta_{pos}) + \\ & \max(0, \Delta_{neg} - d(\tilde{i}_{neg}, \tilde{p}_x))],\end{aligned}\quad (12)$$

where  $\Delta_{pos}$  and  $\Delta_{neg}$  are the positive margin and negative margin.

Fine level descriptor loss is defined as modified circle loss [54]. For each point  $p$ , its positive anchor pixel  $i_{pos}$  and

negative pairs set  $i_{neg}$  are defined as Eq. 11, the descriptor loss is defined as:

$$L_{fine} = \log[1 + \sum_{(p_x, i_y) \in \Omega_{\mathcal{M}}} \exp(\gamma \alpha_{neg}(s(i_{neg}, p_x) - \Delta_{neg})) \exp(-\gamma \alpha_{pos}(s(i_{pos}, p_x) - \Delta_{pos}))], \quad (13)$$

where  $\alpha_{neg}$  and  $\alpha_{pos}$  are the dynamic optimizing rates towards negative and positive pairs, and  $\gamma$  is the scale factor. As in [54], the  $\alpha_{neg}$  and  $\alpha_{pos}$  are defined as:

$$\begin{aligned} \alpha_{neg} &= \max(0, s(i_{neg}, p_x) + \Delta_{neg}), \\ \alpha_{pos} &= \max(0, 1 + \Delta_{pos} - s(i_{pos}, p_x)). \end{aligned} \quad (14)$$

Super-points classification loss is a binary cross-entropy loss:

$$L_{classify} = -\frac{1}{|\tilde{P}|} \sum_{\tilde{p}_x \in \tilde{P}} [\tilde{p}_x \log(\tilde{p}_x^*) + (1 - \tilde{p}_x) \log(1 - \tilde{p}_x^*)]. \quad (15)$$

#### IV. EXPERIMENTS

##### A. Dataset, baseline methods and evaluation metrics

**Dataset:** we evaluate our method on KITTI Odometry dataset [55], a benchmark dataset extensively employed in the field of I2P registration. KITTI Odometry dataset consists of 22 sequences of images and point cloud data collected simultaneously in urban environments, encompassing a variety of road scenes and environmental conditions, and 11 sequences provide ground-truth calibration files. The camera intrinsic function  $\Gamma$  extracted from calibration files is thought unbiased during experiments. For a fair comparison with existing approaches [15, 16], sequences 0-8 are used for training and 9-10 for testing.

**Baseline methods:** we compare proposed CoFiI2P with 2 open-sourced SOTA methods:

- DeepI2P<sup>1</sup> [15]: proposed the frustum classification and inverse camera projection to estimate the camera pose. Due to the time-consuming data pre-processing and training, we reference the registration results of the paper.
- CorrI2P<sup>2</sup> [16]: is SOTA comparable I2P method. CorrI2P [16] predicts the overlapping area and establishes correspondences densely for pose estimation. We use officially released codes to reimplement this method. The only difference is the number of points changed from 40960 to 20480 for fair comparison.

**Evaluation metrics:** we report the relative rotation error (RRE), relative translation error (RTE) and registration recall (RR) to evaluate the registration results. Inlier ratio (IR) and root mean square error (RMSE) used in I2P and P2P approaches [36, 56] are introduced to evaluate the accuracy of correspondences. RRE and RTE are defined as :

$$\begin{aligned} RRE &= \sum_{i=1}^3 |r(i)|, \\ RTE &= \|\mathbf{t}_{gt} - \mathbf{t}_e\|, \end{aligned} \quad (16)$$

where  $r$  is the Euler angle vector of  $\mathbf{R}_{gt}^{-1} \mathbf{R}_E$ ,  $\mathbf{R}_{gt}$  and  $\mathbf{t}_{gt}$  are the ground-truth rotation and translation matrix,  $\mathbf{R}_E$  and  $\mathbf{t}_E$  are the estimated rotation and translation matrix.

RR [36, 56] metrics how many point-to-pixel pairs are correctly estimated, indicating the matching ability of networks. RR is defined as:

$$RR = \frac{1}{|\Omega_{\mathcal{M}^*}|} \sum_{i=1}^{|\Omega_{\mathcal{M}^*}|} \mathbb{1}\left(\sqrt{\frac{1}{|\Omega_{\mathcal{M}^*}|} \sum_{(p_x, i_y) \in \Omega_{\mathcal{M}^*}} \|i_y - \Gamma(\mathbf{T}p_x)\|} < \tau\right), \quad (17)$$

$\tau$  is the threshold to remove false registration results, i.e.  $10^\circ/5m$ .

IR denotes the ratio of linear pairs of matching pairs, which measures the quality of correspondences. The IR for correspondences set  $\Omega_{\mathcal{M}^*}$  is defined as :

$$IR_{\mathcal{M}} = \frac{1}{|\Omega_{\mathcal{M}^*}|} \sum_{(p_x, i_y) \in \Omega_{\mathcal{M}^*}} \mathbb{1}(\|i_y - \Gamma(\mathbf{T}p_x)\| < \tau), \quad (18)$$

in which  $\tau$  is used to control the reprojection error tolerance.

RMSE of image and point cloud ground-truth correspondences  $\Omega_{\mathcal{M}^*}$  is read as:

$$RMSE_{\mathcal{M}} = \sqrt{\frac{1}{|\Omega_{\mathcal{M}^*}|} \sum_{(p_x, i_y) \in \Omega_{\mathcal{M}^*}} \|i_y - \Gamma(\mathbf{T}p_x)\|}. \quad (19)$$

##### B. Implementation Details

Raw images and point clouds are trimmed to filter out noise and reduce the computational burden. The top 50 rows of images are cropped out as most of these pixels see sky. Then images are resized to  $160 \times 512$  for training and testing. The points are downsampled with  $0.1m \times 0.1m \times 0.1m$  voxel and then randomly sampled 20480 points as input. The resolution for coarse matching is 1/8 of original resolution of image and 1/16 of original resolution of point cloud, while 1/2 for both image and point cloud in fine matching.

During the training process, with correct transform parameters provided by the calibration files, the ground truth point-to-pixel correspondences  $\Omega_{\mathcal{M}^*}$  are established to supervise the network. We trained the whole network 25 epochs with batch size of 1. We use the Adam [57] to optimize the network, and the initial learning rate is 0.001 and multiple by 0.25 after every 5 epochs. During training, the safe radius  $r$ , positive margin  $\Delta_{pos}$  and negative margin  $\Delta_{neg}$  are set to 1, 0.2 and 1.8 respectively. Scale factor  $\gamma$  is set to 10. During the coarse matching, super-points are projected to the frustum of image and then we uniformly sample 64 in-frustum super-points. Then, the corresponding super-pixels are found with Eq. 4. For fine matching, we construct a local patch of points/pixels around each seed super-points/super-pixels with point-to-node strategy [58, 59]. During the testing process, to obtain reliable in-frustum super-points in coarse matching, we set the confidence threshold  $\epsilon = 0.9$ .

##### C. Registration Accuracy

Different from [14, 15, 16] which only report conditional RRE and RTE that use thresholds (i.e.  $10^\circ/5m$ ) to reject

<sup>1</sup><https://github.com/liyx10/DeepI2P>

<sup>2</sup><https://github.com/rsy6318/CorrI2P>

TABLE I  
REGISTRATION ACCURACY ON KITTI DATASET

	Threshold( $^{\circ}/m$ )	RRE( $^{\circ}$ )	RTE(m)	RR(%)
DeepI2P (2D)	10/5	$7.56 \pm 7.63$	$3.28 \pm 3.09$	/
DeepI2P (3D)	10/5	$15.52 \pm 12.73$	$3.17 \pm 3.22$	/
	none/none	$7.00 \pm 29.25$	$2.98 \pm 14.30$	/
CorrI2P	45/10	$3.37 \pm 3.61$	$1.48 \pm 1.31$	97.0
	10/5	$2.68 \pm 1.96$	$1.26 \pm 0.85$	90.8
	none/none	$2.52 \pm 4.12(-64\%)$	$0.76 \pm 11.3(-75\%)$	/
CoFiI2P	45/10	$2.44 \pm 2.33(-33\%)$	$0.66 \pm 0.67(-55\%)$	99.8(+2.8)
	10/5	$2.25 \pm 1.68(-14\%)$	$0.61 \pm 0.48(-52\%)$	98.3(+7.5)

false registration frames, we report both conditional and unconditional RRE and RTE of our CoFiI2P, as in Table. I. *none/none* means no thresholds are used to remove false registration frames during evaluation. Our method outperforms all baseline methods by a large margin, which indicates that the CoFiI2P is both robust and accurate in various environments. Specifically, with maximum registration error threshold *none/none*,  $45^{\circ}/10m$ ,  $10^{\circ}/5m$ , the RRE reduces 64%, 33%, 14% and the RTE reduces 75%, 55%, 52% compared to CorrI2P [16] respectively. We indicate that the CorrI2P [16] takes poor performance under large view and illumination variations, but our CoFiI2P operates stably and robustly. Therefore, the global RRE and RTE are significantly better than the CorrI2P [16]. Meanwhile, the RR improves by 2.8%, 7.5% under two pairs of thresholds. Notably, our method significantly improves registration accuracy and reduces inferior results. The qualitative registration results are shown in Fig. 4. We project the points to image plane with transform parameters provided by ground-truth files, CorrI2P [16] and CoFiI2P respectively and render with depth. It can be seen that the CoFiI2P remains stable and provides more accurate results, which proves our indication. More qualitative results are released in the video demo<sup>3</sup>.

**Frustum classification results:** the recall, accuracy and F1-score are shown in Table II. The results show that our CoFiI2P gets higher recall, accuracy and F1-score than CorrI2P [16], where the recall improves about 9.4% over the CorrI2P [16]. The results show that the coarse-to-fine matching schedule excavates more overlapping areas and benefits the pose estimation process.

TABLE II  
FRUSTUM CLASSIFICATION RESULT

method	Recall	Accuracy	F1-score
DeepI2P	/	94.0	/
CorrI2P	89.1	97.1	92.8
CoFiI2P	98.5 (+9.4%)	97.7 (+0.3%)	93.5 (+0.7%)

**Error distribution:** distribution of relative rotation error (RRE) and relative translation error (RTE) on the KITTI dataset are shown in Fig. 6, where the peak of our CoFiI2P is about  $2.5^{\circ}/0.7m$ . Moreover, the predictions of our CoFiI2P

are clearly concentrated in the interval with smaller errors. Neither thresholds nor other constraints are used to remove false registration results.

**IR:** in order to evaluate the quality of correspondences directly, we introduce the inlier ratio (IR) metric as in P2P registration approach [36]. The quantitative results are shown in Fig. 7 and qualitative results are shown in Fig. 5. From Fig. 7, CoFiI2P gets higher IR scores than CorrI2P [16] under different thresholds. As the tolerance threshold increases, the advantage of CoFiI2P becomes more apparent. When the tolerance threshold is set to 5 pixels, IR score of our CoFiI2P is 48.5%, 17.6% higher than CorrI2P [16]; when set to 10 pixels, IR score of CoFiI2P rises to 78.0%, 23.8% higher than CorrI2P [16]. The fact that our method obtains higher IR scores than CorrI2P [16] with a small threshold indicates that the CoFiI2P corrects a large partition of severe misregistration correspondences.

**RMSE:** the RMSE distribution is shown in Fig. 8. From Fig. 8. Specifically, CoFiI2P reduces the global average RMSE value from 25.78 pixels of CorrI2P [16] to 12.97 pixels, about 50.3% improvement. From the pairs matching aspect, our CoFiI2P obviously improves the quality of correspondences in a global view and benefit downstream registration task.

## V. DISCUSSION

In this part, we analyze two crucial modules in our CoFiI2P: I2P transformer and coarse-to-fine matching schedule. We conduct ablation studies on them to prove the effectiveness of each module and review some false cases as well. In order to reduce the computational burden, we train the variant networks 10 epochs in the discussion part, instead of 25 epochs in the experiments part.

### A. I2P transformer

I2P transformer [60] with self-attention module and cross-attention module is crucial for capturing long-range context information. Influence of cross-attention module has been demonstrated in previous approaches, but none of them have discussed the self-attention module. Considering this situation, we conduct ablation studies on the self-attention module. We simply remove all the self-attention modules in I2P transformer (called "CoFiI2P w/o SA"), which means that only cross-attention modules work. Table. III shows the RRE and

<sup>3</sup><https://youtu.be/TG2GBrJTUw4>

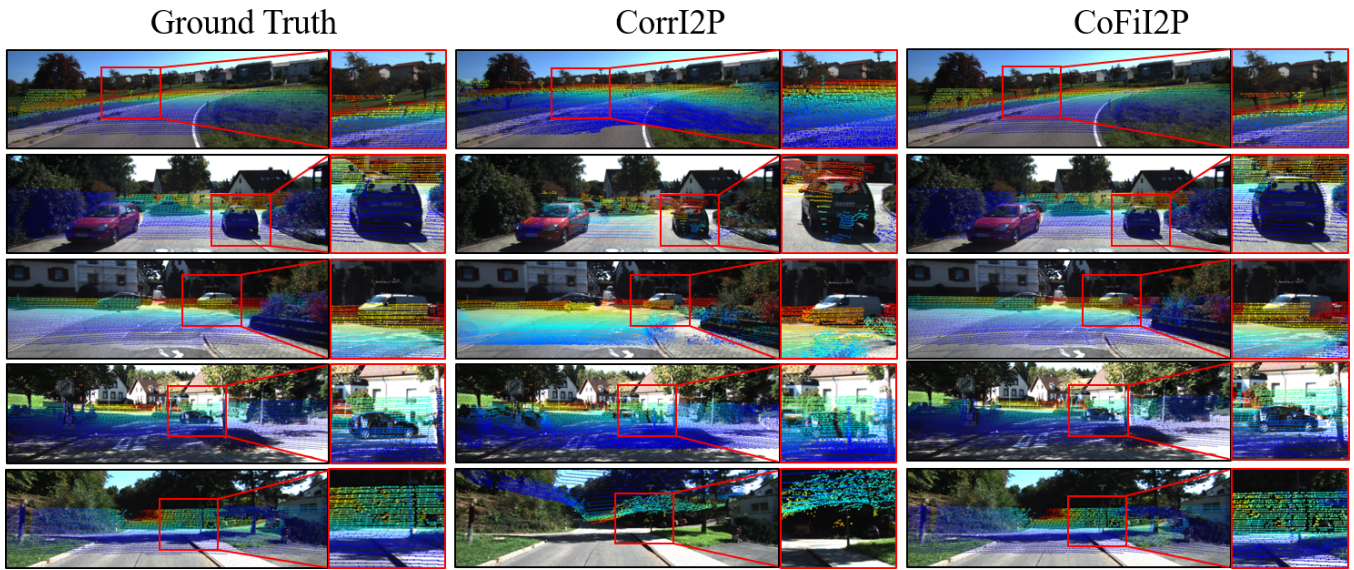


Fig. 4. Quantitative registration results

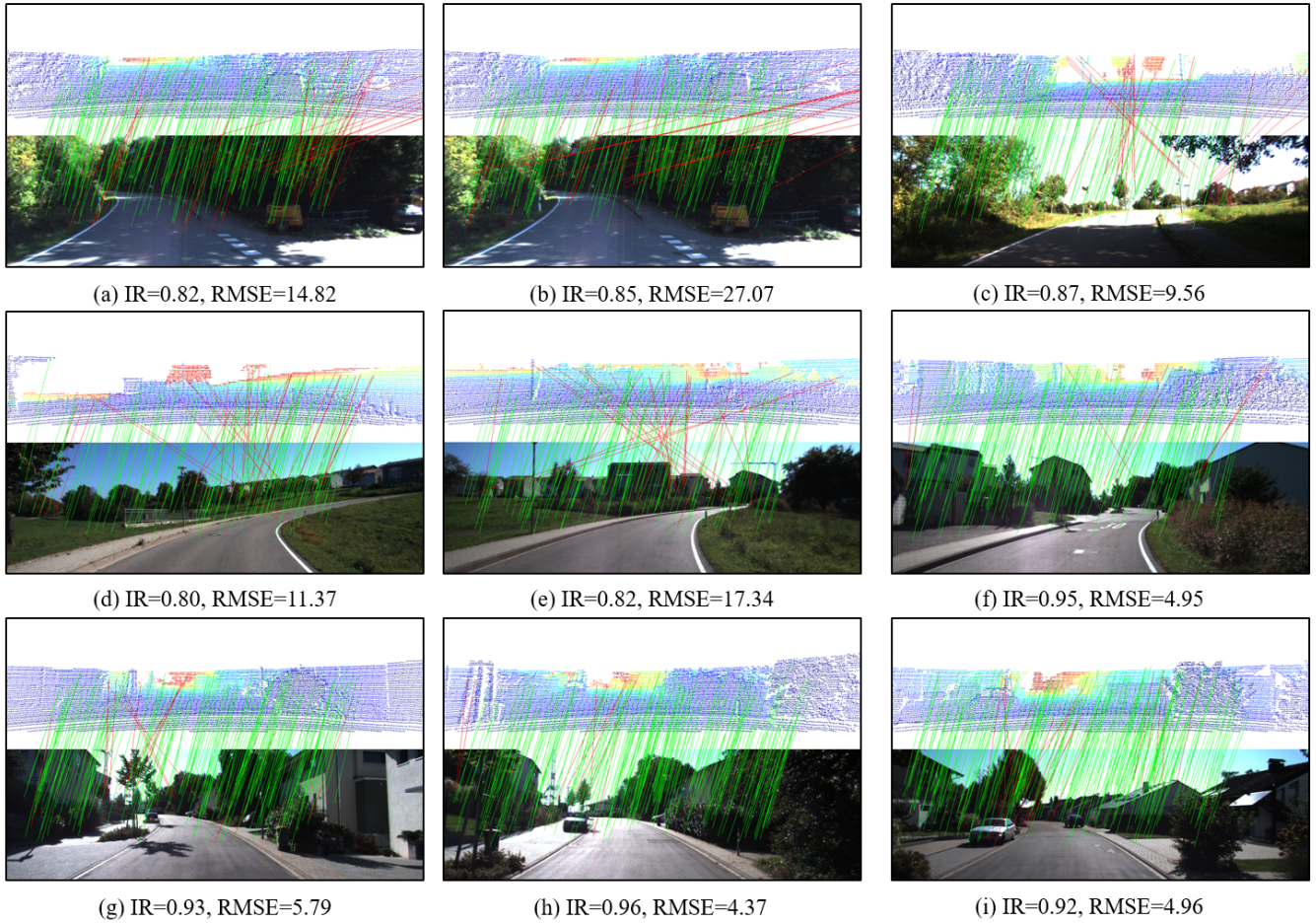


Fig. 5. Qualitative results of correspondences estimated by CoFiI2P

RTE distribution of "CoFiI2P w/o SA". Without the self-attention module in I2P transformer, the conditional and unconditional RRE and RTE degrade remarkably, which means

that the long-range context plays a crucial role in scenario-level I2P registration task.

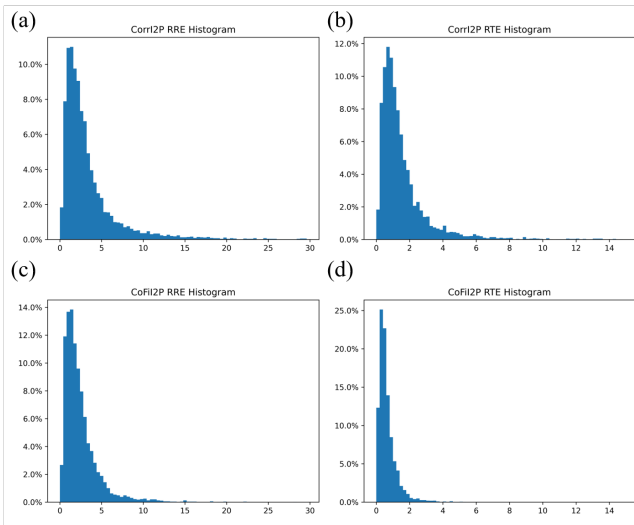


Fig. 6. Error distribution of RRE and RTE. (a) and (b) show the RRE and RTE distribution of CorrI2P [16], and (c) and (d) show the RRE and RTE distribution of CoFiI2P respectively.

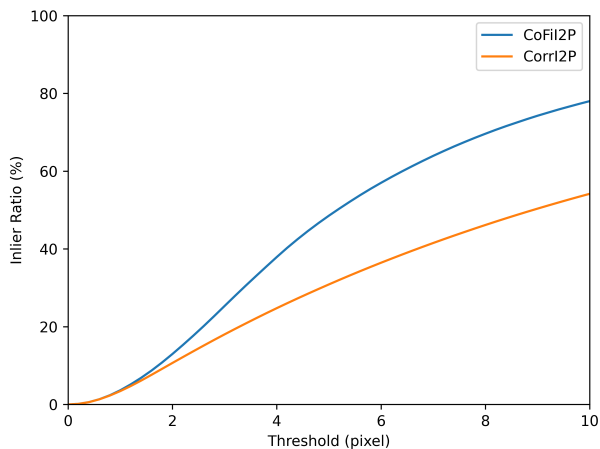


Fig. 7. Comparison of inlier ratio with different thresholds

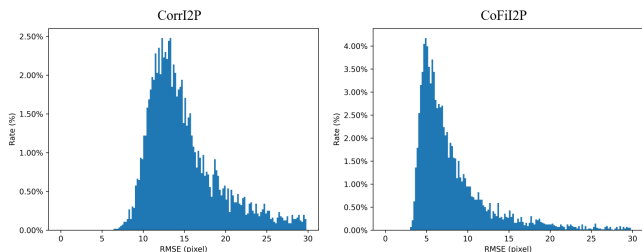


Fig. 8. RMSE distribution of CorrI2P [16] and CoFiI2P

**B. Coarse-to-Fine matching and one-stage matching**

Our CoFiI2P proposes to estimate coarse correspondences at super-point/super-pixel level first and then generate dense correspondences at point-pixel level sequentially. The CoFiI2P is a two-stage registration method, but previous I2P approaches adopt one-stage registration pipeline. To demonstrate that the

progressive two-stage registration operates better than one-stage registration, we conduct two variants of our CoFiI2P network: CoFiI2P-C and CoFiI2P-F. The CoFiI2P-C simply removes the fine matching (FM) module and utilizes the coarse matching results to regress pose. By contrast, the CoFiI2P-F removes the coarse matching (CM) module and estimates correspondences at fine level directly. Table. III shows the registration results of CoFiI2P-C and CoFiI2P-F, where both CoFiI2P-C and CoFiI2P-F get worse regression accuracy and lower registration success rate. Above experiments prove our indication that coarse-level registration provides robust matching pairs and fine-level registration provides accurate matching pairs. Combining the coarse-level and fine-level registration sequentially is beneficial for I2P registration task.

TABLE III  
COMPARISON OF VARIANTS OF CoFiI2P. "CoFiI2P w/o SA" MEANS THE CoFiI2P WITHOUT SELF-ATTENTION MODULES IN THE I2P TRANSFORMER. "CoFiI2P-C" MEANS COARSE MATCHING ONLY AND "CoFiI2P-F" MEANS FINE MATCHING ONLY IN CONTRAST.

method	RRE	RTE
CoFiI2P w/o SA	5.37 ± 7.27	1.78 ± 3.22
CoFiI2P-C	3.39 ± 7.24	0.98 ± 7.22
CoFiI2P-F	3.07 ± 7.73	1.19 ± 14.60
CoFiI2P	<b>2.98 ± 5.41</b>	<b>1.13 ± 13.20</b>

**C. Analysis of false registration case**

The registration accuracy heavily relies on the quality and quantity of extracted features from point cloud and image. Fig. 9 shows 3 cases of false registration scenarios. All of them have common characteristics: 1) lack of distinguishing features; 2) severe mismatching pairs. We suggest that alternative fine registration approaches based on pole matching [40] or road lanes [61] could be supplements of our method in harsh environments.

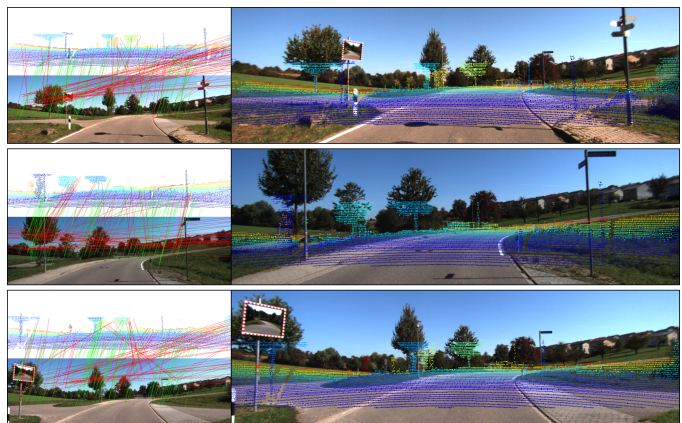


Fig. 9. Example of false registration frames.

**VI. CONCLUSION**

In this paper, we propose CoFiI2P, a novel network for I2P registration. The core is the coarse-to-fine matching strategy, which establishes robust correspondence on the global level

first and learns the precise correspondences on the local level progressively. Furthermore, the I2P transformer with self-attention and cross-attention module is introduced to enhance the global-aware ability in homogeneous and heterogeneous data. Compared with one-stage dense prediction and matching approaches, CoFiI2P filters out a large number of false correspondences and holds a safe lead in all the metrics. Extensive experiments on the KITTI dataset have demonstrated that CoFiI2P owns accuracy, robustness and efficiency in various environments. We hope that our CoFiI2P could motivate the related societies.

In the near future, we intend to design lightweight I2P networks for compact robots and auto-driving vehicles. We believe that real-time transformation parameters regression is crucial for multi-modalities fusion, navigation and downstream perception task.

#### REFERENCES

- [1] D. Shah, B. Osiński, S. Levine *et al.*, “Lm-nav: Robotic navigation with large pre-trained models of language, vision, and action,” in *Conference on Robot Learning*. PMLR, 2023, pp. 492–504.
- [2] N. Tsoi, A. Xiang, P. Yu, S. S. Sohn, G. Schwartz, S. Ramesh, M. Hussein, A. W. Gupta, M. Kapadia, and M. Vázquez, “Sean 2.0: Formalizing and generating social situations for robot navigation,” *IEEE Robotics and Automation Letters*, vol. 7, no. 4, pp. 11 047–11 054, 2022.
- [3] K. Chen, H. Yu, W. Yang, L. Yu, S. Scherer, and G.-S. Xia, “I2d-loc: Camera localization via image to lidar depth flow,” *ISPRS Journal of Photogrammetry and Remote Sensing*, vol. 194, pp. 209–221, 2022.
- [4] C. Chen, B. Wang, C. X. Lu, N. Trigoni, and A. Markham, “Deep learning for visual localization and mapping: A survey,” *arXiv preprint arXiv:2308.14039*, 2023.
- [5] J. Li, B. Yang, C. Chen, R. Huang, Z. Dong, and W. Xiao, “Automatic registration of panoramic image sequence and mobile laser scanning data using semantic features,” *ISPRS Journal of Photogrammetry and Remote Sensing*, vol. 136, pp. 41–57, 2018.
- [6] Y. Liu, M.-M. Cheng, D.-P. Fan, L. Zhang, J.-W. Bian, and D. Tao, “Semantic edge detection with diverse deep supervision,” *International Journal of Computer Vision*, vol. 130, no. 1, pp. 179–198, 2022.
- [7] Y. Chen, J. Liu, X. Zhang, X. Qi, and J. Jia, “Voxel-next: Fully sparse voxelnet for 3d object detection and tracking,” in *Proceedings of the IEEE/CVF Conference on Computer Vision and Pattern Recognition*, 2023, pp. 21 674–21 683.
- [8] L. Nunes, L. Wiesmann, R. Marcuzzi, X. Chen, J. Behley, and C. Stachniss, “Temporal consistent 3d lidar representation learning for semantic perception in autonomous driving,” in *Proceedings of the IEEE/CVF Conference on Computer Vision and Pattern Recognition*, 2023, pp. 5217–5228.
- [9] A. Milioto, I. Vizzo, J. Behley, and C. Stachniss, “Rangenet++: Fast and accurate lidar semantic segmentation,” in *2019 IEEE/RSJ international conference on intelligent robots and systems (IROS)*. IEEE, 2019, pp. 4213–4220.
- [10] R. Qin, J. Tian, and P. Reinartz, “3d change detection—approaches and applications,” *ISPRS Journal of Photogrammetry and Remote Sensing*, vol. 122, pp. 41–56, 2016.
- [11] X. Zhang, S. Zhu, S. Guo, J. Li, and H. Liu, “Line-based automatic extrinsic calibration of lidar and camera,” in *2021 IEEE International Conference on Robotics and Automation (ICRA)*. IEEE, 2021, pp. 9347–9353.
- [12] S. Wang, X. Zhang, G. Zhang, Y. Xiong, G. Tian, S. Guo, J. Li, P. Lu, J. Wei, and L. Tian, “Temporal and spatial online integrated calibration for camera and lidar,” in *2022 IEEE 25th International Conference on Intelligent Transportation Systems (ITSC)*. IEEE, 2022, pp. 3016–3022.
- [13] C. Yuan, X. Liu, X. Hong, and F. Zhang, “Pixel-level extrinsic self calibration of high resolution lidar and camera in targetless environments,” *IEEE Robotics and Automation Letters*, vol. 6, no. 4, pp. 7517–7524, 2021.
- [14] M. Feng, S. Hu, M. H. Ang, and G. H. Lee, “2d3d-matchnet: Learning to match keypoints across 2d image and 3d point cloud,” in *2019 International Conference on Robotics and Automation (ICRA)*. IEEE, 2019, pp. 4790–4796.
- [15] J. Li and G. H. Lee, “Deepi2p: Image-to-point cloud registration via deep classification,” in *Proceedings of the IEEE/CVF Conference on Computer Vision and Pattern Recognition*, 2021, pp. 15 960–15 969.
- [16] S. Ren, Y. Zeng, J. Hou, and X. Chen, “Corri2p: Deep image-to-point cloud registration via dense correspondence,” *IEEE Transactions on Circuits and Systems for Video Technology*, vol. 33, no. 3, pp. 1198–1208, 2022.
- [17] D. G. Lowe, “Distinctive image features from scale-invariant keypoints,” *International journal of computer vision*, vol. 60, pp. 91–110, 2004.
- [18] Y. Zhong, “Intrinsic shape signatures: A shape descriptor for 3d object recognition,” in *2009 IEEE 12th international conference on computer vision workshops, ICCV Workshops*. IEEE, 2009, pp. 689–696.
- [19] J. Sun, Z. Shen, Y. Wang, H. Bao, and X. Zhou, “Loftr: Detector-free local feature matching with transformers,” in *Proceedings of the IEEE/CVF conference on computer vision and pattern recognition*, 2021, pp. 8922–8931.
- [20] W. Jiang, E. Trulls, J. Hosang, A. Tagliasacchi, and K. M. Yi, “Cotr: Correspondence transformer for matching across images,” in *Proceedings of the IEEE/CVF International Conference on Computer Vision*, 2021, pp. 6207–6217.
- [21] Z. Qin, H. Yu, C. Wang, Y. Guo, Y. Peng, and K. Xu, “Geometric transformer for fast and robust point cloud registration,” in *Proceedings of the IEEE/CVF conference on computer vision and pattern recognition*, 2022, pp. 11 143–11 152.
- [22] H. Wang, Y. Liu, Q. Hu, B. Wang, J. Chen, Z. Dong, Y. Guo, W. Wang, and B. Yang, “Roreg: Pairwise point cloud registration with oriented descriptors and local

- rotations,” *IEEE Transactions on Pattern Analysis and Machine Intelligence*, 2023.
- [23] O. Ronneberger, P. Fischer, and T. Brox, “U-net: Convolutional networks for biomedical image segmentation,” in *Medical Image Computing and Computer-Assisted Intervention—MICCAI 2015: 18th International Conference, Munich, Germany, October 5–9, 2015, Proceedings, Part III* 18. Springer, 2015, pp. 234–241.
- [24] V. Lepetit, F. Moreno-Noguer, and P. Fua, “Ep n p: An accurate o (n) solution to the p n p problem,” *International journal of computer vision*, vol. 81, pp. 155–166, 2009.
- [25] M. A. Fischler and R. C. Bolles, “Random sample consensus: a paradigm for model fitting with applications to image analysis and automated cartography,” *Communications of the ACM*, vol. 24, no. 6, pp. 381–395, 1981.
- [26] E. Rublee, V. Rabaud, K. Konolige, and G. Bradski, “Orb: An efficient alternative to sift or surf,” in *2011 International conference on computer vision*. Ieee, 2011, pp. 2564–2571.
- [27] D. DeTone, T. Malisiewicz, and A. Rabinovich, “Toward geometric deep slam,” *arXiv preprint arXiv:1707.07410*, 2017.
- [28] DeTone, Daniel and Malisiewicz, Tomasz and Rabinovich, Andrew, “Superpoint: Self-supervised interest point detection and description,” in *Proceedings of the IEEE conference on computer vision and pattern recognition workshops*, 2018, pp. 224–236.
- [29] P.-E. Sarlin, D. DeTone, T. Malisiewicz, and A. Rabinovich, “Superglue: Learning feature matching with graph neural networks,” in *Proceedings of the IEEE/CVF conference on computer vision and pattern recognition*, 2020, pp. 4938–4947.
- [30] Q. Zhou, T. Sattler, and L. Leal-Taixe, “Patch2pix: Epipolar-guided pixel-level correspondences,” in *Proceedings of the IEEE/CVF conference on computer vision and pattern recognition*, 2021, pp. 4669–4678.
- [31] H. Deng, T. Birdal, and S. Ilic, “Ppf-foldnet: Unsupervised learning of rotation invariant 3d local descriptors,” in *Proceedings of the European conference on computer vision (ECCV)*, 2018, pp. 602–618.
- [32] H. Wang, Y. Liu, Z. Dong, and W. Wang, “You only hypothesize once: Point cloud registration with rotation-equivariant descriptors,” in *Proceedings of the 30th ACM International Conference on Multimedia*, 2022, pp. 1630–1641.
- [33] Z. Gojcic, C. Zhou, J. D. Wegner, and A. Wieser, “The perfect match: 3d point cloud matching with smoothed densities,” in *Proceedings of the IEEE/CVF conference on computer vision and pattern recognition*, 2019, pp. 5545–5554.
- [34] H. Yu, Z. Qin, J. Hou, M. Saleh, D. Li, B. Busam, and S. Ilic, “Rotation-invariant transformer for point cloud matching,” in *Proceedings of the IEEE/CVF Conference on Computer Vision and Pattern Recognition*, 2023, pp. 5384–5393.
- [35] S. Ao, Q. Hu, H. Wang, K. Xu, and Y. Guo, “Buffer: Balancing accuracy, efficiency, and generalizability in point cloud registration,” in *Proceedings of the IEEE/CVF Conference on Computer Vision and Pattern Recognition*, 2023, pp. 1255–1264.
- [36] H. Yu, F. Li, M. Saleh, B. Busam, and S. Ilic, “Cofinet: Reliable coarse-to-fine correspondences for robust point-cloud registration,” *Advances in Neural Information Processing Systems*, vol. 34, pp. 23 872–23 884, 2021.
- [37] Z. J. Yew and G. H. Lee, “Regtr: End-to-end point cloud correspondences with transformers,” in *Proceedings of the IEEE/CVF conference on computer vision and pattern recognition*, 2022, pp. 6677–6686.
- [38] S. Huang, Z. Gojcic, M. Usvatsov, A. Wieser, and K. Schindler, “Predator: Registration of 3d point clouds with low overlap,” in *Proceedings of the IEEE/CVF Conference on computer vision and pattern recognition*, 2021, pp. 4267–4276.
- [39] J. Levinson and S. Thrun, “Automatic online calibration of cameras and lasers,” in *Robotics: science and systems*, vol. 2, no. 7. Citeseer, 2013.
- [40] Y. Wang, Y. Li, Y. Chen, M. Peng, H. Li, B. Yang, C. Chen, and Z. Dong, “Automatic registration of point cloud and panoramic images in urban scenes based on pole matching,” *International Journal of Applied Earth Observation and Geoinformation*, vol. 115, p. 103083, 2022.
- [41] Y. Liao, J. Li, S. Kang, Q. Li, G. Zhu, S. Yuan, Z. Dong, and B. Yang, “Se-calib: Semantic edges based lidar-camera boresight online calibration in urban scenes,” *IEEE Transactions on Geoscience and Remote Sensing*, 2023.
- [42] Q. Zhang and R. Pless, “Extrinsic calibration of a camera and laser range finder (improves camera calibration),” in *2004 IEEE/RSJ International Conference on Intelligent Robots and Systems (IROS)(IEEE Cat. No. 04CH37566)*, vol. 3. IEEE, 2004, pp. 2301–2306.
- [43] R. Unnikrishnan and M. Hebert, “Fast extrinsic calibration of a laser rangefinder to a camera,” *Robotics Institute, Pittsburgh, PA, Tech. Rep. CMU-RI-TR-05-09*, 2005.
- [44] D. Scaramuzza, A. Harati, and R. Siegwart, “Extrinsic self calibration of a camera and a 3d laser range finder from natural scenes,” in *2007 IEEE/RSJ International Conference on Intelligent Robots and Systems*. IEEE, 2007, pp. 4164–4169.
- [45] I. Stamos, L. Liu, C. Chen, G. Wolberg, G. Yu, and S. Zokai, “Integrating automated range registration with multiview geometry for the photorealistic modeling of large-scale scenes,” *International Journal of Computer Vision*, vol. 78, pp. 237–260, 2008.
- [46] G. Pandey, J. McBride, S. Savarese, and R. Eustice, “Automatic targetless extrinsic calibration of a 3d lidar and camera by maximizing mutual information,” in *Proceedings of the AAAI Conference on Artificial Intelligence*, vol. 26, no. 1, 2012, pp. 2053–2059.
- [47] K. He, X. Zhang, S. Ren, and J. Sun, “Deep residual learning for image recognition,” in *Proceedings of the IEEE conference on computer vision and pattern recognition*, 2016, pp. 770–778.

- [48] H. Thomas, C. R. Qi, J.-E. Deschaud, B. Marcotegui, F. Goulette, and L. J. Guibas, “Kpconv: Flexible and deformable convolution for point clouds,” in *Proceedings of the IEEE/CVF international conference on computer vision*, 2019, pp. 6411–6420.
- [49] C. Choy, J. Gwak, and S. Savarese, “4d spatio-temporal convnets: Minkowski convolutional neural networks,” in *Proceedings of the IEEE/CVF conference on computer vision and pattern recognition*, 2019, pp. 3075–3084.
- [50] Z. Zhou, M. M. R. Siddiquee, N. Tajbakhsh, and J. Liang, “Unet++: Redesigning skip connections to exploit multi-scale features in image segmentation,” *IEEE transactions on medical imaging*, vol. 39, no. 6, pp. 1856–1867, 2019.
- [51] W. Zhang, Z. Huang, G. Luo, T. Chen, X. Wang, W. Liu, G. Yu, and C. Shen, “Topformer: Token pyramid transformer for mobile semantic segmentation,” in *Proceedings of the IEEE/CVF Conference on Computer Vision and Pattern Recognition*, 2022, pp. 12 083–12 093.
- [52] Q. Wan, Z. Huang, J. Lu, G. Yu, and L. Zhang, “Seaformer: Squeeze-enhanced axial transformer for mobile semantic segmentation,” *arXiv preprint arXiv:2301.13156*, 2023.
- [53] K. Wu, H. Peng, M. Chen, J. Fu, and H. Chao, “Re-thinking and improving relative position encoding for vision transformer,” in *Proceedings of the IEEE/CVF International Conference on Computer Vision*, 2021, pp. 10 033–10 041.
- [54] Y. Sun, C. Cheng, Y. Zhang, C. Zhang, L. Zheng, Z. Wang, and Y. Wei, “Circle loss: A unified perspective of pair similarity optimization,” in *Proceedings of the IEEE/CVF conference on computer vision and pattern recognition*, 2020, pp. 6398–6407.
- [55] A. Geiger, P. Lenz, and R. Urtasun, “Are we ready for autonomous driving? the kitti vision benchmark suite,” in *2012 IEEE conference on computer vision and pattern recognition*. IEEE, 2012, pp. 3354–3361.
- [56] B. Wang, C. Chen, Z. Cui, J. Qin, C. X. Lu, Z. Yu, P. Zhao, Z. Dong, F. Zhu, N. Trigoni *et al.*, “P2-net: Joint description and detection of local features for pixel and point matching,” in *Proceedings of the IEEE/CVF International Conference on Computer Vision*, 2021, pp. 16 004–16 013.
- [57] D. P. Kingma and J. Ba, “Adam: A method for stochastic optimization,” *arXiv preprint arXiv:1412.6980*, 2014.
- [58] C. R. Qi, L. Yi, H. Su, and L. J. Guibas, “Pointnet++: Deep hierarchical feature learning on point sets in a metric space,” *Advances in neural information processing systems*, vol. 30, 2017.
- [59] J. Li, B. M. Chen, and G. H. Lee, “So-net: Self-organizing network for point cloud analysis,” in *Proceedings of the IEEE conference on computer vision and pattern recognition*, 2018, pp. 9397–9406.
- [60] A. Dosovitskiy, L. Beyer, A. Kolesnikov, D. Weissenborn, X. Zhai, T. Unterthiner, M. Dehghani, M. Minderer, G. Heigold, S. Gelly *et al.*, “An image is worth 16x16 words: Transformers for image recognition at scale,” *arXiv preprint arXiv:2010.11929*, 2020.
- [61] T. Ma, Z. Liu, G. Yan, and Y. Li, “Crlf: Automatic calibration and refinement based on line feature for lidar and camera in road scenes,” *arXiv preprint arXiv:2103.04558*, 2021.